Supporting Information

Formation of Stable Strontium-Rich Amorphous Calcium Phosphate: Possible Effects on Bone Mineral

Camila B. Tovani[†¶*], *Alexandre Gloter*[‡], *Thierry Azaïs*[†], *Mohamed Selmane*[§], *Ana P. Ramos*[¶], *Nadine Nassif*[†*]

[†]Sorbonne Université, CNRS, Collège de France, Laboratoire Chimie de la Matière Condensée de Paris, 4 Place Jussieu, F-75005 Paris, France

[‡]Université Paris Sud, Laboratoire de Physique des Solides, CNRS UMR 8502, F-91405 Orsay, France

[§]Institut des Matériaux de Paris Centre, IMPC, Univ Paris 06, Collège de France, 11 place Marcelin Berthelot, F-75231 Paris, France

[¶]Departamento de Química, Faculdade de Filosofia, Ciências e Letras de Ribeirão Preto, Universidade de São Paulo, Ribeirão Preto 14040-901, SP, Brazil

* Corresponding authors: Camila B. Tovani and Dr. Nadine Nassif

Table S1. Sr^{2+} molar percentages (% Sr^{2+}) in relation to the total number of mols of divalent cations (Ca^{2+} + Sr^{2+}) in the starting solutions and in the products determined by SEM-EDX

%Sr^{2+} in the solution	**%Sr^{2+} in the product**
0	0
5	3±1
10	10±1
25	20±1
50	40±2
75	60±2
100	100

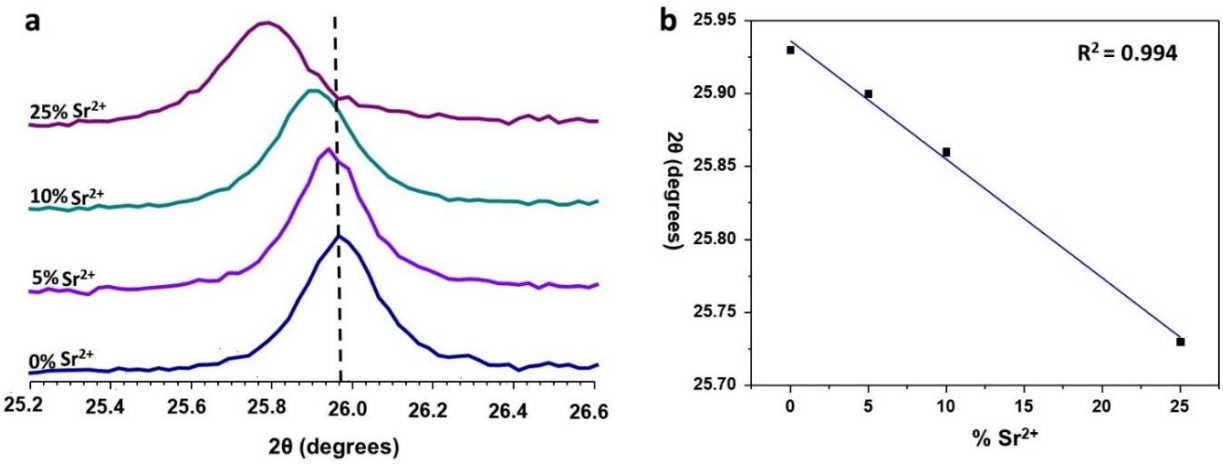

Figure S1. (a) Enlarged XRD patterns of the series of samples 0-25% Sr^{2+} showing the displacement of the 002 peak to lower 2θ values upon increasing Sr^{2+} content in the samples. (b) Position of the 002 peaks as a function of % Sr^{2+}.

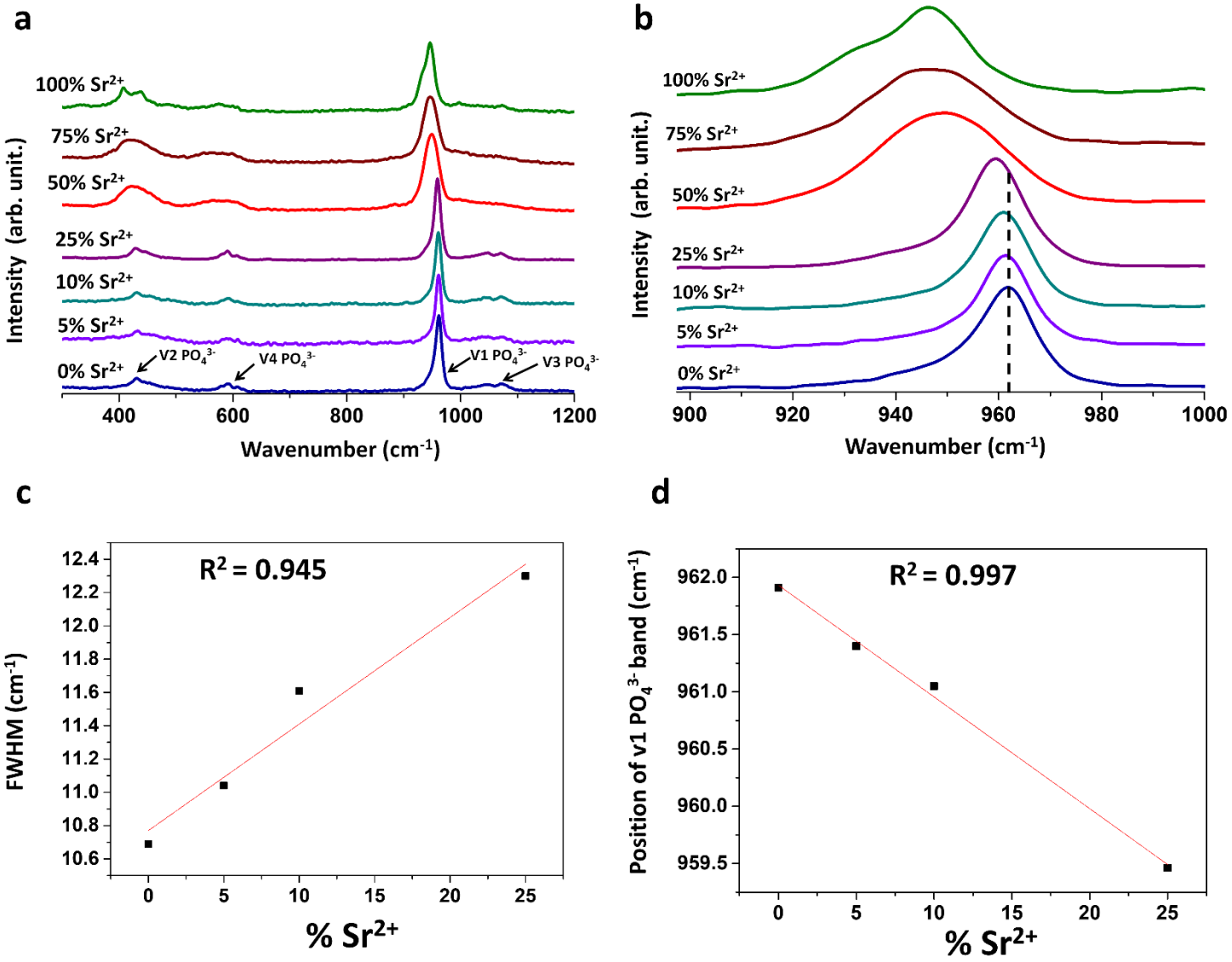

Figure S2. (a) Raman spectra of the series of samples 0-100% Sr^{2+} (b) Enlarged V1 PO_4^{3-} Raman bands showing the broadening and displacement of the band upon increasing Sr^{2+} content. (c) Correlation between the FWHM values of the V1 PO_4^{3-} Raman band and $\%Sr^{2+}$. (d) Correlation between the V1 PO_4^{3-} Raman band position as function of $\%Sr^{2}$.

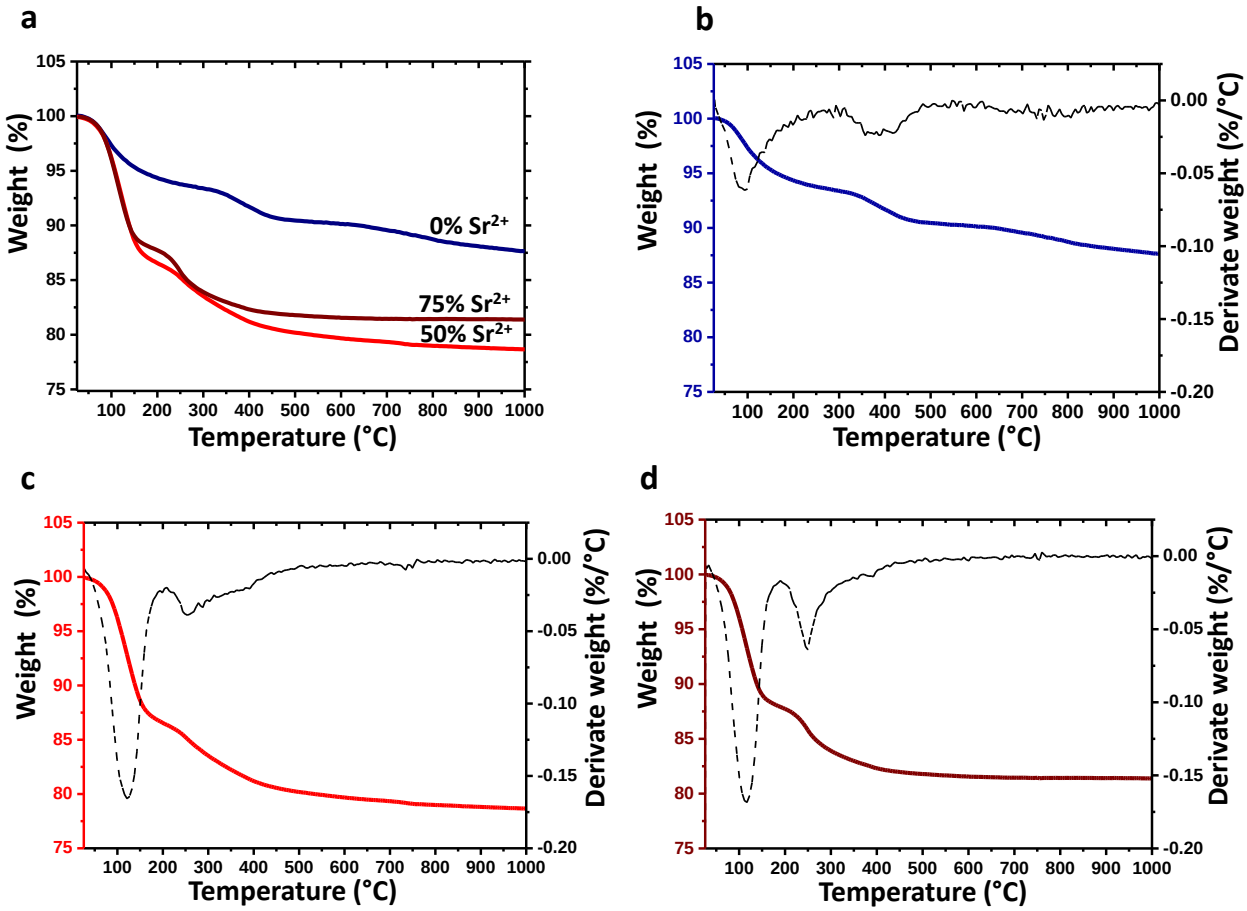

Figure S3. (a) TGA curves of the 0% Sr^{2+}, 50% Sr^{2+} and 75% Sr^{2+} samples and (b, c and d) thermogravimetry (left axis) and differential thermogravimetry (dashed black curve, right axis) of the 0% Sr^{2+},50% Sr^{2+} and 75% Sr^{2+} samples respectively. The TGA curves display two loss events in the range of 25-400°C related to the dehydration process. Adsorbed (surface) water molecules are released in the 25-200 °C range and structural water in the 200-400 °C range. The total weight loss of water estimated to the 0% Sr^{2+}, 50% Sr^{2+} and 75% Sr^{2+} samples is 9.8 wt%, 18.9 wt% and 16.6 wt% respectively.

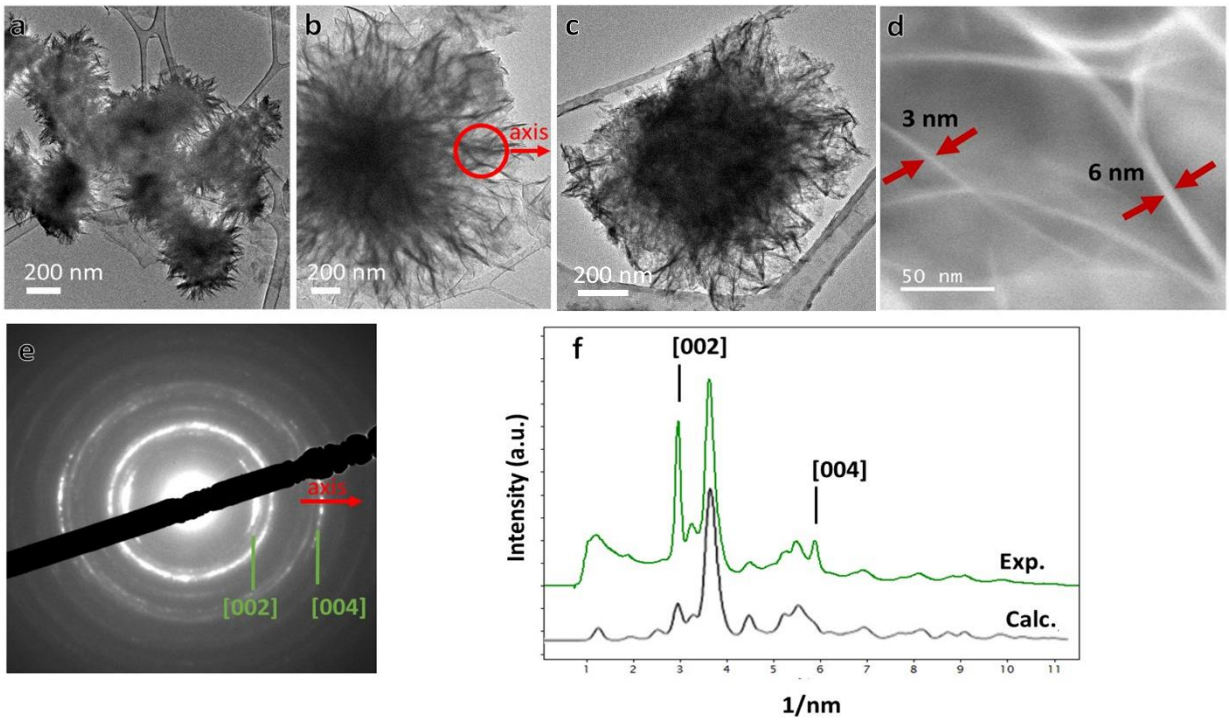

Figure S4. (a-c) TEM images of the 0% Sr^{2+}, 5% Sr^{2+} and 25% Sr^{2+} samples. (d) STEM-HAADF image of 25% Sr^{2+} samples showing crystalline thin leaves composed of slabs of 3-6 nm of thickness. (e) SAED from the encircled area of the 5% Sr^{2+} sample. The orientation of the SAED with respect to the image is indicated by the radial axis. SAED exhibits a (002) planes preferential radial orientation. (f) Radial integration of the SAED of (e) and the calculation for isotropic electron diffraction of HA. The preferential growth direction results in a stronger (002) and (004) planes contributions in the experimental curve.

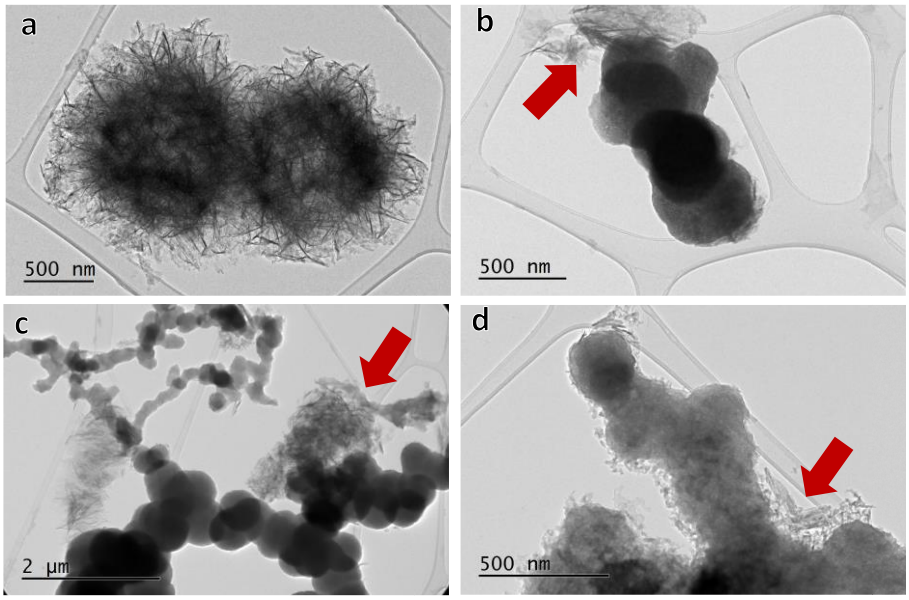

Figure S5. TEM images of the 25%Sr^{2+} sample showing (a) HA and (b-d) amorphous particles. The presence of apatitic particles (indicated by red arrows) surrounding the amorphous aggregates suggests that the latter can be converted into HA. The coexistence of amorphous and apatitic structures highlights the saturation of HA with respect to %Sr^{2+}.

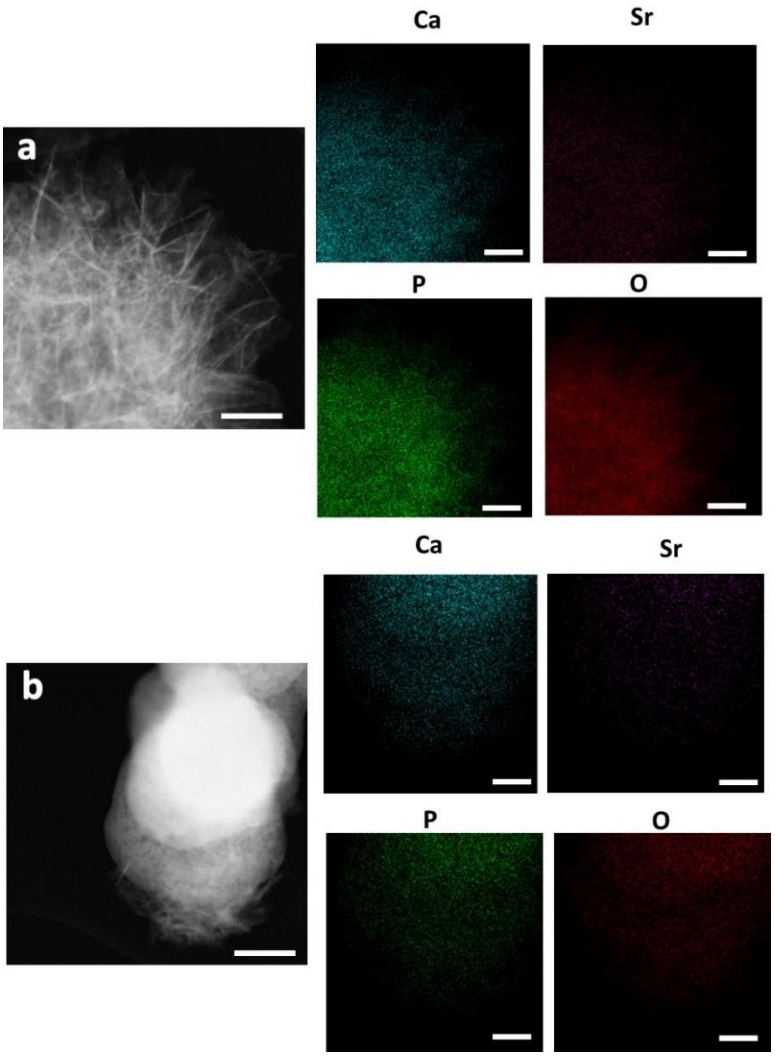

Figure S6. TEM images and EDS mapping of the 25%Sr^{2+} sample showing the distribution of Sr, Ca, P, and O over the apatitic (a) and amorphous (b) particles. Scale bar in all panels is 200 nm.

Table S2. ^{31}P chemical shifts (δ) and line widths (LW) obtained from quantitative ^{31}P NMR spectra

Sample	**δ(^{31}P) ±0.05 ppm**	**LW ±10 Hz**
0% Sr^{2+}	2.76	200
5% Sr^{2+}	2.87	200
10% Sr^{2+}	2.90	227
25% Sr^{2+}	3.05	300
50% Sr^{2+}	2.80	614
75% Sr^{2+}	3.20	630

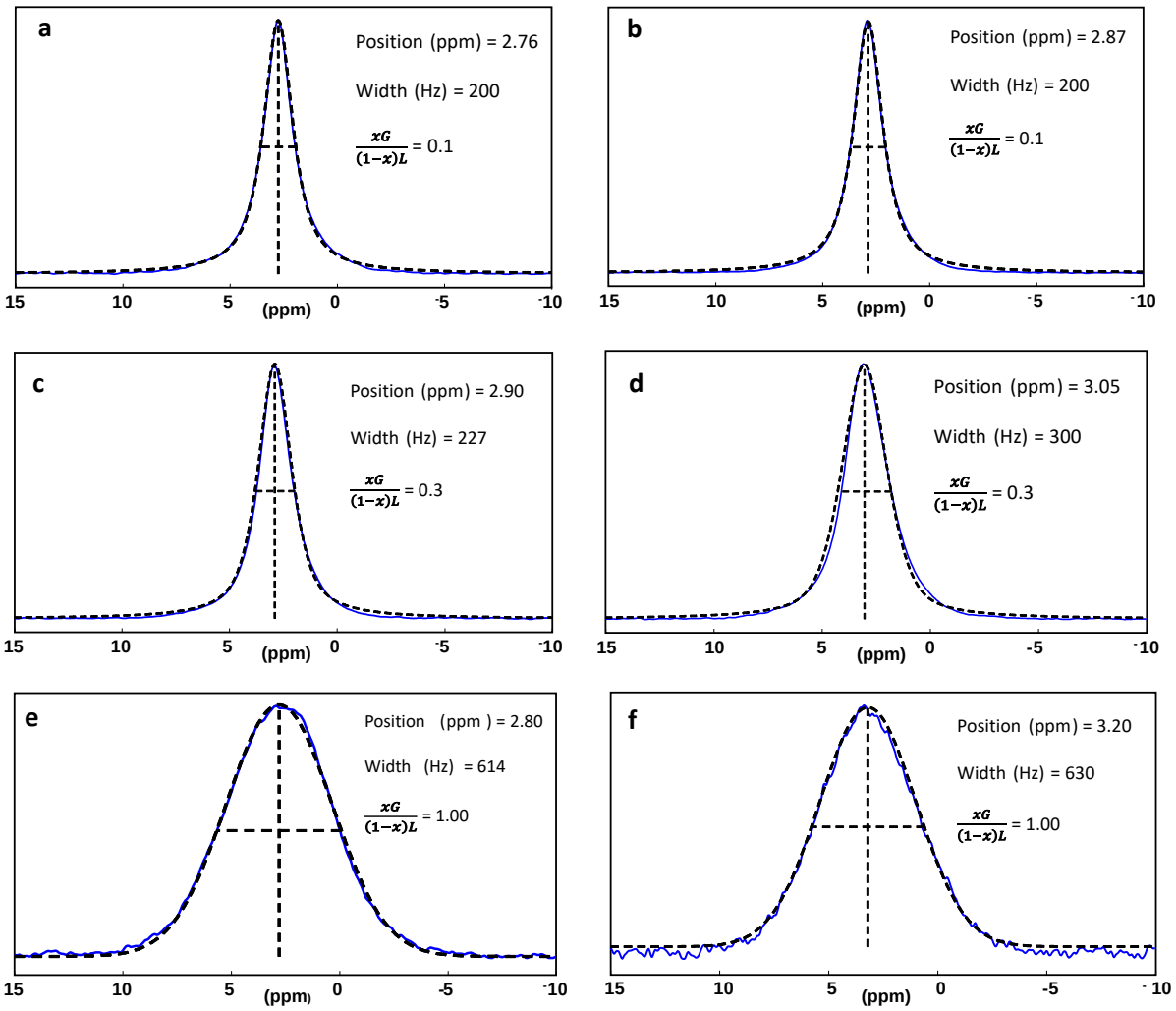

Figure S7. ^{31}PMAS spectra (blue line) with the line fitting (black dashed line) of the samples (a) 0% Sr^{2+}; (b) 5% $Sr^{2+;}$ (c) 10% Sr^{2+}; (d) 25% Sr^{2+}; (e) 50% Sr^{2+} and (f) 75% Sr^{2+}. The extracted parameters peak position and line width and are displayed in ppm and Hz respectively. It can be observed that the Gaussian fraction $\frac{xG}{(1-X)L}$ increases with the Sr^{2+} content in the samples confirming the increase of the distribution of environments around the phosphates.

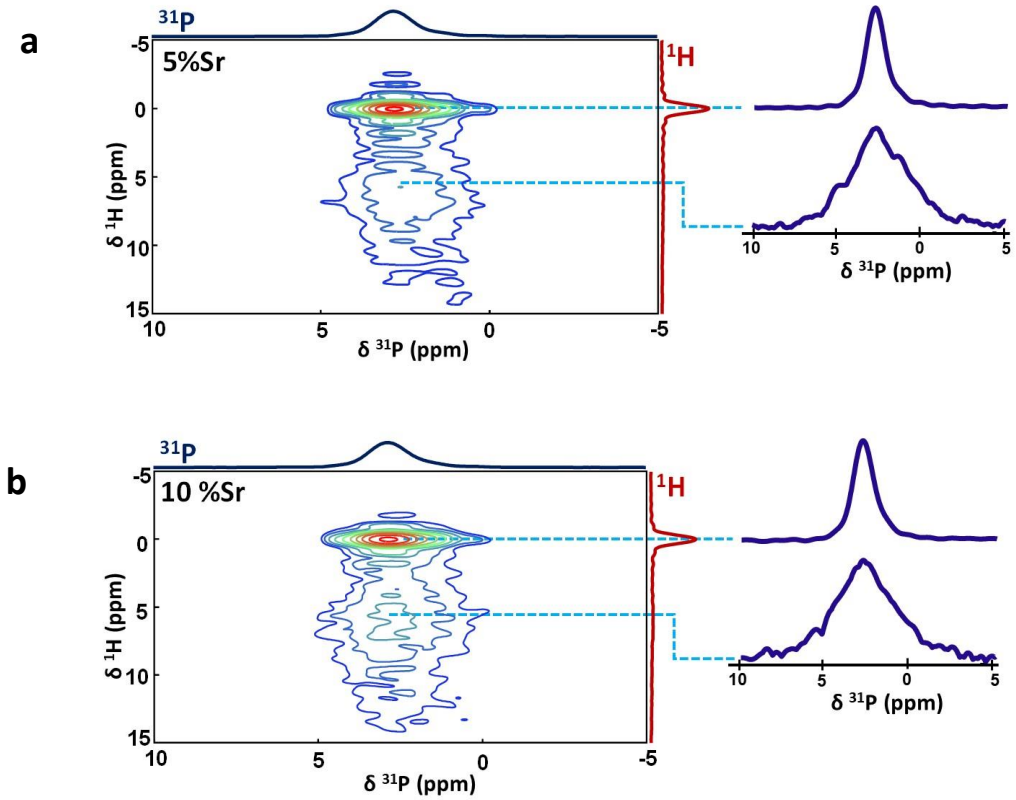

Figure S8. ^{1}H-^{31}P HetCor spectra of the 5%Sr^{2+} and 10%Sr^{2+}samples and extracted ^{31}P slices corresponding to the resonance at δ(^{1} H) = 0 and 4.85 ppm.

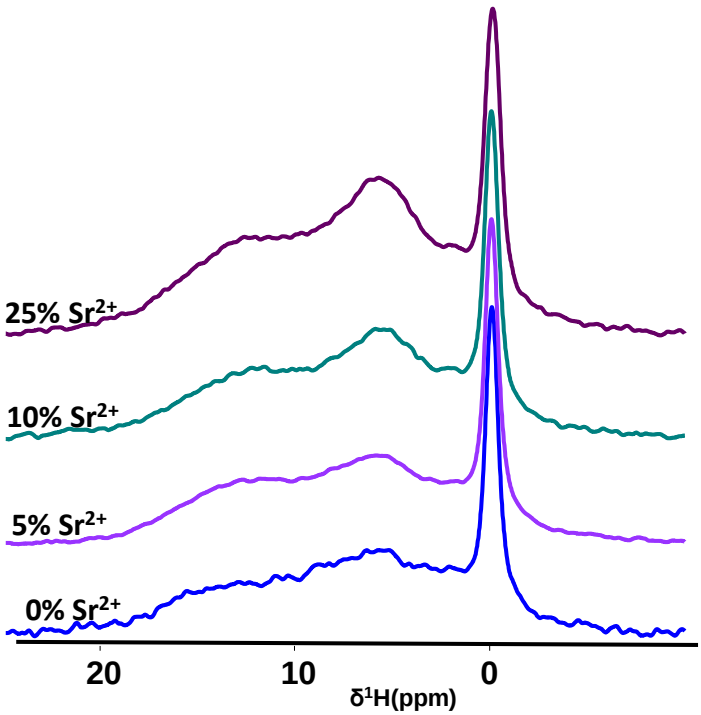

Figure S9. Double CP $^{1}H \rightarrow ^{31}P \rightarrow ^{1}H$ MAS NMR spectra of the series of samples 0-25%Sr^{2+}.

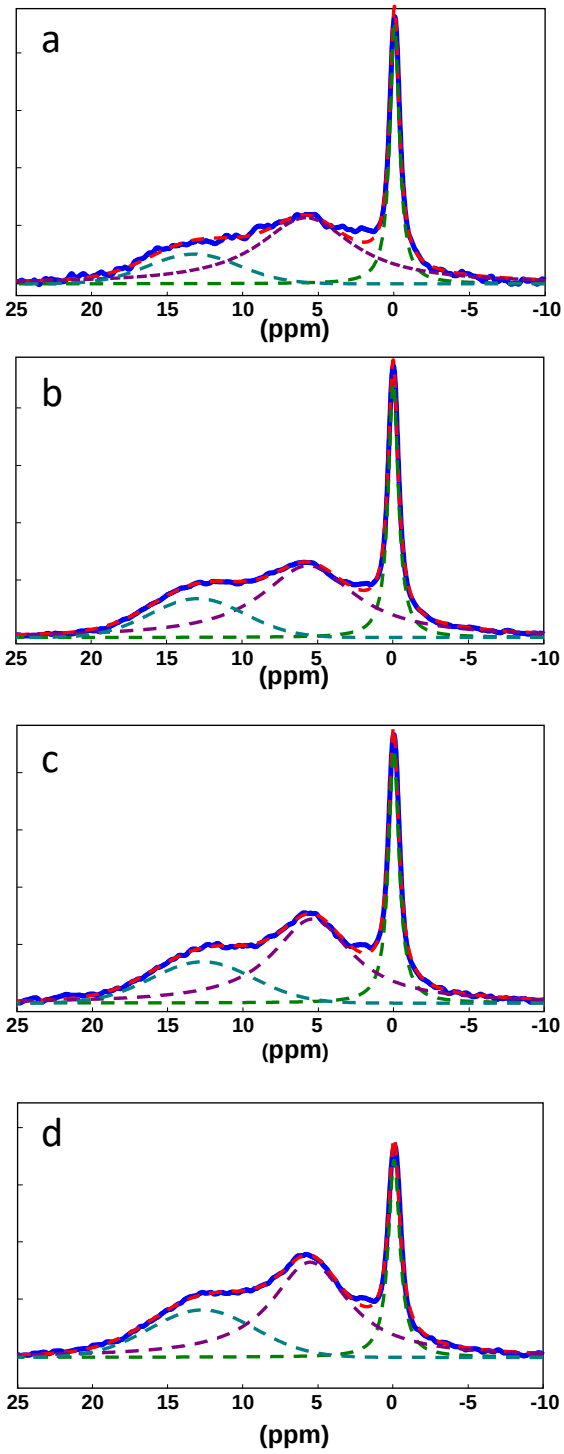

Figure S10. Double CP $^{1}H \rightarrow ^{31}P \rightarrow ^{1}H$ MAS NMR spectra (blue line) of the series of samples 0% Sr^{2+} (a); 5% Sr^{2+} (b); 10% Sr^{2+} (c) and 25% Sr^{2+}(d), with the line fitting (dashed lines) of the peaks around 0 ppm which is characteristic of OH^{-} ions in the crystalline apatitic environment, and two peaks, centered at 5.5 and 12.5 ppm, corresponding to adsorbed water and HPO_4^{2-}, respectively.